

Star formation and gas flow history of a dwarf irregular galaxy traced by gas-phase and stellar metallicities

Nao Fukagawa^{1,2}★

¹*The Graduate University for Advanced Studies, SOKENDAI, 2-21-1 Osawa, Mitaka, Tokyo, 181-8588, Japan*

²*Tohoku University, 6-3 Aramaki, Aoba-ku, Sendai, Miyagi, 980-8578, Japan*

Accepted XXX. Received YYY; in original form ZZZ

ABSTRACT

Studying the evolution of dwarf galaxies can provide insights into the characteristics of systems that can act as building blocks of massive galaxies. This paper discusses the history of star formation and gas flows (inflow and outflow) of a dwarf irregular galaxy in the Local Group, NGC 6822, from the viewpoint of gas-phase and stellar chemical abundance. Gas-phase oxygen abundance, stellar metallicity distribution and gas fraction data are compared to chemical evolution models in which continuous star formation and gas flows are assumed. If the galaxy is assumed to be a closed or an accretion-dominated system where steeper stellar initial mass functions are allowed, the observed gas-phase oxygen abundance and gas fraction can be explained simultaneously; however metallicity distributions predicted by the models seem to be inconsistent with the observed distribution, which suggests that the star formation, gas flows and/or chemical enrichment are more complex than assumed by the models. When NGC 6822 is assumed to be a system dominated by outflow, the observed values of gas-phase oxygen abundance and gas fraction can be explained, and the metallicity distributions predicted by some of the models are also roughly consistent with the observed distribution in the metallicity range of $-2.0 \lesssim [\text{Fe}/\text{H}] \lesssim -0.5$. It should be noted that this result does not necessarily mean that the accretion of gas is completely ruled out. More observables, such as chemical abundance ratios, and detailed modelling may provide deeper insight into the evolution of the system.

Key words: galaxies: dwarf

1 INTRODUCTION

It is important to study how dwarf galaxies evolve, because small systems are the building blocks of larger systems in the framework of the hierarchical merging scenario. Each dwarf galaxy has its own star formation history (Mateo 1998; Tolstoy, Hill & Tosi 2009). When supernovae inject sufficient energy to blow the interstellar gas away, a dwarf galaxy may lose material to form stars. The accretion of gas or gas-rich systems may also have an influence on star formation. Investigating the evolution of individual star-forming dwarf galaxies can provide insight into understanding the variation in star formation history of dwarf galaxies.

Metallicity is a fundamental property that provides information about the evolution of galaxies. Interstellar gas turns into stars, which produce heavy elements and then return their gas and the synthesized elements into the interstellar medium. Stars in subsequent generations are formed from gas enriched by previous generations. Galaxies may

also acquire and/or lose gas. The accretion of low-metallicity gas on to a galaxy may temporarily decrease the gas-phase metallicity. The outflow triggered by supernovae carries part of the gas, including heavy elements, out of the galaxy. Therefore, chemical abundances trace the histories of star formation and gas flows of galaxies.

There have been many studies on the chemical evolution of nearby star-forming dwarf galaxies, including dwarf irregular galaxies and blue compact dwarf galaxies, based on gas-phase abundances (Pagel 1997; Tosi 1998; Matteucci 2012, references therein). These studies explain the abundances of star-forming dwarf galaxies mainly by the stellar initial mass function (IMF) for the solar neighbourhood or steeper IMFs with which less-massive stars are formed more frequently, galactic wind and/or discontinuous star formation. For some dwarf irregular galaxies in the Local Group, individual stars are resolved, and stellar abundances are measured from the spectra (e.g. Venn et al. 2001; Tautvaišienė et al. 2007). Metallicity distributions, from which the histories of star formation and gas flows are obtained, and the evolution of individual galaxies are discussed by comparing the observed

★ E-mail: nao.fukagawa@nao.ac.jp

distribution with analytical chemical evolution models (e.g. Kirby et al. 2013; Leaman et al. 2013).

The histories of the star formation and gas flows of dwarf irregular galaxies are discussed from both sides of gas-phase and stellar metallicities, but the observational data can be explained by models with different assumptions (Tosi 1998), which brings about different suggestions. What can be inferred about the evolution of dwarf irregular galaxies from both of gas-phase and stellar metallicities with unique models? In addition to sophisticated models and simulations (e.g. Revaz & Jablonka 2018), models with a small number of assumptions also provide insight into the dominant physical processes.

Within this context, this paper investigates the evolution of a dwarf irregular galaxy by comparing the gas-phase oxygen abundance, gas fraction and metallicity distribution to chemical evolution models. Among the dwarf irregular galaxies in the Local Group, this work focuses on NGC 6822. This galaxy is one of the nearest dwarf irregular galaxies to the Milky Way (~ 460 kpc; McConnachie 2012, references therein). The stellar mass ($1 \times 10^8 M_{\odot}$; McConnachie 2012, references therein) is about one-fifth as large as that of the Small Magellanic Cloud, but NGC 6822 is located in a more isolated environment (Mateo 1998). The gas mass is almost comparable to the stellar mass ($M_{\text{HI}} = 1.34 \times 10^8 M_{\odot}$; de Blok & Walter 2006). The integrated star formation rate, as measured using H α images, is $0.01 M_{\odot} \text{ yr}^{-1}$ (Hunter & Elmegreen 2004), and a recent increase in the star formation rate has been reported (e.g. Cannon et al. 2012). The gas-phase oxygen abundance has been measured for H II regions (e.g. Skillman, Terlevich & Melnick 1989; Lee et al. 2006; Peimbert, Peimbert & Ruiz 2005) and planetary nebulae (e.g. Richer & McCall 2007; Hernández-Martínez et al. 2009). The measured value is around $0.2\text{--}0.4 Z_{\text{O},\odot}$ ¹, and may vary depending on the measurement method. There is not clear evidence for the abundance gradient (e.g. Lee et al. 2006) and the gas of the galaxy is homogeneous (e.g. Hernández-Martínez et al. 2009) within 2 kpc radius from the centre. Stellar abundances have also been investigated by observing supergiants (e.g. Muschelok et al. 1999; Venn et al. 2001; Patrick et al. 2015), globular clusters (e.g. Colucci, Bernstein & McWilliam 2010; Larsen et al. 2018) and red giants (e.g. Tolstoy et al. 2001; Kirby et al. 2013; Swan et al. 2016).

The literature discusses the chemical history of NGC 6822 based on gas-phase abundances with chemical evolution models. For example, Carigi, Colín & Peimbert (2006) and Hernández-Martínez et al. (2011) discussed the chemical evolution of NGC 6822 by comparing data on gas-phase abundances and abundance ratios to the models in which the suppression of gas accretion due to reionization is assumed. In these papers, the authors suggested the need to consider outflow. The metallicity distribution has also been studied using models. Kirby et al. (2013) showed that the shape of the observed metallicity distribution can be explained by an

analytical model in which outflow is dominant, and a small amount of the gas accretes into the galaxy. They also suggested that most of the iron produced by stars has been lost from NGC 6822, based on the yields of supernovae and gas-phase and stellar abundances. Hartwick (2015) explained the shape of the distribution using a model taking gas accretion and multiple small starbursts into account, and interpreted the result as star formation may be repeatedly ignited by merging with gas-rich systems or at intersections of streams of gas.

The present study considers both sides of the gas-phase and stellar metallicities using chemical evolution models in which gas accretion or outflow is assumed to dominate the system. The structure of this paper is as follows: observational data of NGC 6822 compared to models are summarized in Section 2; details of the models are described in Section 3; observational data are compared to the models in Section 4; and a summary and discussion are presented in Section 5.

2 OBSERVATIONAL DATA

In this study, gas-phase oxygen abundance, metallicity distribution and gas mass fraction reported previously are compared to model predictions.

The gas-phase oxygen abundance (Z_{O}) is based on the value measured by Lee et al. (2006). They measured chemical abundances of nebulae at radii $\lesssim 2$ kpc based on the intensities of emission lines. The temperature-sensitive [O III] $\lambda 4363$ line was detected for five H II regions and the abundances were derived by the direct method. They did not find clear evidence for the abundance gradient. Assuming zero slope of the gradient, they took the average oxygen abundances of the five H II regions. In the present study, the value $Z_{\text{O}} = 8.11 \pm 0.11$ is considered to be the average gas-phase oxygen abundance of NGC 6822. The value scaled to the solar abundance (Asplund et al. 2004) is $Z_{\text{O}}/Z_{\text{O},\odot} = 0.28 \pm 0.06$.

The stellar metallicity distribution is taken from a spectroscopic study conducted by Kirby et al. (2013). They measured the metallicities ($[\text{Fe}/\text{H}]$) of individual red giant stars in NGC 6822 using a method based on spectral synthesis. The metallicity distribution consists of 276 stars. The typical error of the metallicity of the stars is $\langle \delta[\text{Fe}/\text{H}] \rangle = 0.13$. The mean metallicity is $\langle [\text{Fe}/\text{H}] \rangle = -1.05 \pm 0.01$. The distribution shows that the measured metallicity ranges from $[\text{Fe}/\text{H}] \sim -3.1$ to 0, which suggests that some of the member stars have Fe abundances as high as the sun, while the average gas-phase oxygen abundance is about 30 per cent of the solar abundance. It has been reported that the mean oxygen abundance or global metallicity of supergiant stars in NGC 6822 agree with that of H II regions (for the oxygen abundance, $Z_{\text{O}} = 8.36 \pm 0.19$ (Venn et al. 2001), and for the global metallicity, $\log Z/Z_{\odot} = -0.52 \pm 0.21$ (Patrick et al. 2015)). Because red giants are older than supergiants, low metallicities of red giants can be interpreted as they have been formed from low-metallicity gas where the chemical enrichment has not proceeded yet. However, the existence of the metal rich red giant stars cannot be explained by the scenario alone. Although evidence is lacking, one possible explanation of the origin of the Fe-rich stars is that they formed from gas en-

¹ In this study, chemical abundances are represented by $Z_{\text{A}} = 12 + \log(\text{A}/\text{H})$ and $[\text{A}/\text{B}] = \log(\text{A}/\text{B}) - \log(\text{A}/\text{B})_{\odot}$, where A and B are abundances of elements A and B. If not otherwise specified, $[\text{Fe}/\text{H}]$ is considered to be the stellar metallicity.

riched by supernova(e) before the gas had been well mixed. It is also possible that stars in other systems have accreted on to NGC 6822. This point should be examined in future studies.

With regard to the chemical abundances, stellar abundance ratios give insight into the chemical enrichment of galaxies. The α -elements, in which oxygen included, are mainly produced by massive stars, and the Fe-peak elements can also be produced by type-Ia supernovae. $[\alpha/\text{Fe}]$ of stars in NGC 6822 has been measured for several globular clusters (e.g. Larsen et al. 2018) and A-type supergiants (Venn et al. 2001). Currently, the observational data about stellar abundance ratios may not be sufficient to compare them with models and constrain the star formation history. The observed stellar abundance ratios of dwarf irregular galaxies will help to understand their evolution.

The gas mass fraction (μ) is defined as the fraction of gas ($\text{H I} + \text{H}_2$) mass to the sum of gas and stellar masses. For the H I gas, de Blok & Walter (2006) measured H I flux and derived H I gas mass. Their observations covered an area of $4^\circ \times 4^\circ$. The derived H I gas mass is $M_{\text{HI}} = 1.34 \times 10^8 M_\odot$. The H_2 gas mass is taken from a study by Israel (1997), who suggested $M_{\text{H}_2} = 1.5(+3, -1) \times 10^7 M_\odot$ based on $^{12}\text{CO}(J = 1 - 0)$ brightness. For the stellar mass, assuming a mass-to-luminosity ratio of unity, McConnachie (2012, references therein) derived the stellar mass of NGC 6822. The value is $M_* = 1 \times 10^8 M_\odot$. The gas mass fraction based on these gas and stellar masses is 0.6. The region investigated may not always be consistent among these papers. In the present study, the value of the gas mass fraction is considered to be representative of NGC 6822.

3 CHEMICAL EVOLUTION MODELS

Observational data described in the previous section are compared to three one-zone numerical models. These models are constructed according to Prantzos (2008). The assumptions are summarized in the following sections.

In this work, it is assumed that the gas is instantaneously mixed and homogeneous (one-zone model), and that stars are formed continuously. Of course, this assumption may be too simple to completely reproduce the observed quantities of NGC 6822. With regard to assumptions about star formation, time variation in the star formation rate can be derived using photometric data (Carigi, Colín & Peimbert 2006). However, galaxies evolve through the interplay of star formation, gas accretion and outflow. The fluctuation in star formation rate may result in temporal changes in the rates of gas accretion and outflow, which could influence subsequent star formation activity. Although including assumptions about this fluctuation is important, it requires additional parameters in the models. In general, the star formation activity appears to be continuing (Cannon et al. 2012; Weisz et al. 2014). In addition, galaxies of larger mass may have more continuous star formation histories compared to galaxies of lower masses (e.g. Weisz et al. 2012). Assuming continuous star formation may not be completely against the point that NGC 6822 is a relatively massive dwarf galaxy.

Chemical abundances and physical properties are calculated in the time range of $t = 0.00 - 13.80$ Gyr with intervals

of 0.01 Gyr. Previous studies (e.g. Fusco et al. 2014) yielded evidence that there are stars older than 10 Gyr in NGC 6822. Based on the presence of the old stellar populations, the observed values of gas-phase oxygen abundance and gas mass fraction are compared to predicted values in the universe at present ($t = 13.80$ Gyr).

The interstellar gas in NGC 6822 involves a small amount of dust ($M_{\text{dust}} = 1.4 \times 10^4 M_\odot$; Israel, Bontekoe & Kester 1996). Thus, a fraction of the elements in the interstellar gas is probably captured in the dust, but the degree of dust depletion in low-metallicity gas is not clear. In this study, no assumptions about dust depletion are included in the models.

All calculations are performed in reduced mass scaled to the total mass of the system. The parameters of the models are summarised in Table 1.

3.1 Closed-box model (model A)

A galaxy is assumed to evolve as a closed system of gas mass $M_g(M_\odot)$ and stellar mass $M_*(M_\odot)$. There is no exchange of gas with the outer region. The total mass of the system $M_{\text{total}}(M_\odot)$ is given by $M_{\text{total}} = M_g + M_*$. The evolution of gas mass and stellar mass can be described as follows:

$$\frac{dM_g(t)}{dt} = -\Psi(t) + E_g(t), \quad (1)$$

$$\frac{dM_*(t)}{dt} = \Psi(t) - E_g(t), \quad (2)$$

where $\Psi(t)$ and $E_g(t)$ are the star formation rate and the rate of gas ejected by dying stars at time t (Gyr), respectively. The star formation rate is assumed to be

$$\Psi(t) = k_{\text{SF}} M_g(t), \quad (3)$$

where k_{SF} is a constant referred to as the star formation efficiency (SFE). The initial mass function $\Phi(M)$ is:

$$\Phi(M) \propto M^{-(1+x)}, \quad (4)$$

where x is the index. In the case of the Salpeter IMF (Salpeter 1955), $x = 1.35$. The IMF is normalized as follows:

$$\Phi(M) = A \int_{M_L}^{M_U} \Phi(M) M dM = 1, \quad (5)$$

where A is a normalization constant. In this study, the lower and upper limits of masses of stars M_L and M_U are assumed to be $M_L = 0.08 M_\odot$ and $M_U = 50 M_\odot$, respectively. Stars more massive than $50 M_\odot$ may be formed in dwarf galaxies. The upper mass of $50 M_\odot$ is set in view of the mass range provided in tables of supernova yield (Nomoto, Kobayashi & Tominaga 2013).

The rate of mass ejection of dying stars at time t (Gyr) is

$$E_g(t) = \int_{M_t}^{M_U} (M - C_M) \Psi(t - \tau_M) \Phi(M) dM, \quad (6)$$

where M_t (M_\odot) represents the mass of stars whose lifetime corresponds to the age of the system. For stellar lifetime τ_M (Gyr), the theoretical values provided by Schaller et al. (1992) are adopted. With regard to the mass of stellar remnants C_M (M_\odot), it is assumed that stars of mass $M/M_\odot < 9$,

Table 1. Summary of chemical evolution models. f_g, f_* and $f_{g,h}$ representing mass fractions: $f_g = M_g/M_{\text{total}}$, $f_* = M_*/M_{\text{total}}$ and $f_{g,h} = M_{g,h}/M_{\text{total}}$.

model	parameter(s)	infall rate (Gyr ⁻¹)	outflow rate (Gyr ⁻¹)	initial condition
A	k_{SF}	–	–	$f_g = 1, f_* = 0, Z_{\text{O}} = 0, Z_{\text{Fe}} = 0$
B	$k_{\text{SF}}, k_{\text{in}}$	$F(t) = k_{\text{in}} M_{g,h}$	–	$f_{g,h} = 1, f_g = 0, f_* = 0, Z_{\text{O}} = 0, Z_{\text{Fe}} = 0$
C	k_{SF}, η	–	$O(t) = \eta \Psi(t)$	$f_{g,h} = 0, f_g = 1, f_* = 0, Z_{\text{O}} = 0, Z_{\text{Fe}} = 0$

$9 < M/M_{\odot} < 25$ and $25 < M/M_{\odot}$ leave white dwarfs, neutron stars and black holes, respectively:

$$C_M = \begin{cases} 0.08M + 0.47 & (M/M_{\odot} < 9) \\ 1.35 & (9 < M/M_{\odot} < 25) \\ 0.24M - 4 & (25 < M/M_{\odot}). \end{cases} \quad (7)$$

With regard to chemical enrichment, the evolution of the mass of element i is:

$$\frac{d(M_g X_i)}{dt} = -\Psi(t) X_i(t) + E_i(t), \quad (8)$$

where $X_i(t)$ is the mass fraction of element i and $E_i(t)$ is the rate of ejection of element i . Massive stars produce large amounts of α -elements through type-II supernovae (SNe II), and type-Ia supernovae (SNe Ia) contribute to the enrichment of Fe-peak elements. Low- and intermediate-mass stars also contribute to the enrichment of some elements (e.g. carbon and nitrogen). In this study, gas-phase oxygen abundance and metallicity distribution are compared, and it is assumed that chemical abundances are mainly changed by SNe II and SNe Ia:

$$E_i(t) = E_{i,\text{II}}(t) + E_{i,\text{Ia}}(t), \quad (9)$$

where $E_{i,\text{II}}(t)$ and $E_{i,\text{Ia}}(t)$ are the rates of ejection of mass of element i by SNe II and SNe Ia, respectively. For SNe II,

$$E_{i,\text{II}}(t) = \int_{M_i}^{M_U} \{y_i + X_i(t - \tau_M)(M - C_M - y_i)\} \Psi(t - \tau_M) \Phi(M) dM. \quad (10)$$

The first bracket shows the amount of element i ejected by a star and $y_i(M_{\odot})$ represents the amount of element i newly produced by the star. In this study, the metallicity-dependent yields of SNe II ($Z = 0, 0.001, 0.004, 0.008, 0.02$ and 0.05) provided by [Nomoto, Kobayashi & Tominaga \(2013\)](#) are adopted. They take the mass loss of stars into account in the calculation. A contribution to chemical enrichment by hypernovae is not assumed in the present study. For SNe Ia, it is assumed that a proportion of stars of $3-8 M_{\odot}$ are binary and explode τ_{Ia} Gyr after formation. The rate of ejection of element i by SNe Ia is described as follows:

$$E_{i,\text{Ia}} = f_{\text{Ia}} \int_{3M_{\odot}}^{8M_{\odot}} y_{i,\text{Ia}} \Phi(M) \Psi(t - \tau_{\text{Ia}}) dM, \quad (11)$$

where $y_{i,\text{Ia}} (M_{\odot})$ is the yield ([Nomoto et al. 1997](#)). The fraction f_{Ia} and lifetime τ_{Ia} (Gyr) are determined to be $f_{\text{Ia}} = 0.05$ and $\tau_{\text{Ia}} = 2.0$ (Gyr), respectively, based on a comparison between the infall model (model B) and abundances of stars in the Milky Way. The details are explained in the Appendix A. Predicted metallicity distributions in this work are convolved with an error function on the assumption that observational data include uncertainty (set to 0.1 dex as a typical value). When SNe Ia start to contribute to chemical enrichment (2 Gyr after star formation starts in the

galaxy), the abundance of Fe begins to increase sharply. This effect makes the metallicity distributions from the models discontinuous, resulting in the overproduction of stars on the metal-poor side of the distributions. The overproduction is particularly clear for models A and C, in which the accretion of gas is not taken into account. The simple assumption regarding the enrichment by SNe Ia partly causes the overproduction, and in this work the shape of the main peak of the distributions is compared to the observational data.

3.2 Infall model (model B)

A galaxy is assumed to be a system in which the accretion of primordial gas dominates. Part of the metal-free gas in the gas reservoir accretes into the galaxy. In contrast to model A in which a galaxy is assumed to be formed from a gas cloud, in model B, the gas is provided from the gas reservoir to the main body. Thus, the gas mass and star formation rate increase with time in the early stage of the evolution. The total mass of the system is $M_{\text{total}} = M_g + M_* + M_{g,h}$, where $M_{g,h}(M_{\odot})$ represents the gas mass of the reservoir. The evolution of the mass of gas, stars and element i in the galaxy is described as follows:

$$\frac{dM_g}{dt} = -\Psi(t) + E_g(t) + F(t), \quad (12)$$

$$\frac{dM_*}{dt} = \Psi(t) - E_g(t), \quad (13)$$

$$\frac{d(M_g X_i)}{dt} = -\Psi(t) X_i(t) + E_i(t). \quad (14)$$

The infall rate $F(t)$ is simply assumed to be proportional to the gas mass in the reservoir:

$$F(t) = k_{\text{in}} M_{g,h}(t). \quad (15)$$

The coefficient k_{in} is a constant referred to as the accretion efficiency (ACE). k_{in} in this model and η in model C may depend on other physical quantities, such as time (e.g. [Carigi, Colín & Peimbert 2006](#); [Lian et al. 2018](#)), but this dependence is still a matter of some debate. In this study, these quantities are assumed to be constants. The investigated ranges of the SFE and ACE are $k_{\text{SF}} = 0.010 - 0.090$ (Gyr⁻¹) and $k_{\text{in}} = 0.010 - 0.90$ (Gyr⁻¹), respectively. Other assumptions are the same as those of model A.

3.3 Outflow model (model C)

A galaxy is considered an outflow-dominated system. Part of the interstellar gas, including heavy elements, is expelled due to galactic wind accompanying supernovae. Thus, the outflow rate $O(t)$ is assumed to be proportional to the star formation rate ([Hartwick 1976](#)): $O(t) = \eta \Psi(t)$, where η is

a constant referred to as the mass-loading factor. It is assumed that the ejecta of supernovae are mixed with the interstellar medium before the outflow and that the chemical abundances of the outflowing gas are equal to those of the interstellar gas of the galaxy at time t . The total mass of the system is $M_{\text{total}} = M_{\text{g}} + M_{\text{*}} + M_{\text{out}}$, where M_{out} (M_{\odot}) is the mass of gas ejected from the galaxy. The evolution is described as follows:

$$\frac{dM_{\text{g}}}{dt} = -\Psi(t) + E_{\text{g}}(t) - O(t), \quad (16)$$

$$\frac{dM_{\text{*}}}{dt} = \Psi(t) - E_{\text{g}}(t), \quad (17)$$

$$\frac{d(M_{\text{g}} X_i)}{dt} = -\Psi(t) X_i(t) + E_i(t) - O(t) X_i(t). \quad (18)$$

Other assumptions are the same as those of model A.

4 COMPARING THE OBSERVATIONAL DATA WITH MODELS

4.1 Closed system

It is assumed that NGC 6822 is a closed system. The properties are compared to model A.

Firstly, star formation is assumed to obey the IMF for the solar neighbourhood, and the Salpeter IMF (Salpeter 1955, $x = 1.35$) is adopted. Fig. 1 shows the observational data and predictions of the models for different SFEs. Fig. 1a shows the metallicity distributions. According to the analytical solution of the closed-box model, metallicity depends on the gas fraction and yield (e.g. Pagel 1997). The differences in metallicity at the peak of metallicity distributions ($[\text{Fe}/\text{H}]_{\text{peak}}$) in Fig. 1a are due to low SFE. Fig. 1b shows the μ - Z_{O} diagram. The curves are evolutionary tracks of galaxies predicted by the models. The gas turns into stars and the stars produce heavy elements, so galaxies evolve along the curve from left to right on this plane. Points on the curves show the gas-phase oxygen abundance and the gas mass fraction in the universe at present. Galaxies of higher SFE consume gas more rapidly by star formation, so they have a smaller gas mass fraction at any given time. They also have higher gas-phase oxygen abundance at any given time, because a large amount of oxygen is produced by SNeII. Galaxies evolve along almost self-similar tracks on the μ - Z_{O} diagram, regardless of the SFE.

The gaseous properties and metallicity distribution seem not to be explained simultaneously with model A. Regarding the gas-phase oxygen abundance and gas mass fraction, the gas-phase oxygen abundance predicted by model A is high compared to the observed value at the gas mass fraction of NGC 6822 ($\mu = 0.6$). For example, a gas mass fraction in a model of $k_{\text{SF}} = 0.050$ (Gyr^{-1}) (yellow curve in Fig. 1b) is almost consistent with the observed value of gas mass fraction, but this model predicts gas-phase oxygen abundance of $Z_{\text{O}}/Z_{\text{O},\odot} \sim 0.6$, while the observed value is $Z_{\text{O}}/Z_{\text{O},\odot} \sim 0.3$. Thus, the observed low gas-phase oxygen abundance cannot be explained only by assuming different SFEs. These results do not conflict with those of previous studies (e.g. Matteucci & Chiosi 1983). In light of stellar and gas-phase abundances, Fig. 1 suggests that $[\text{Fe}/\text{H}]_{\text{peak}}$ and gas-phase oxygen abundance of NGC 6822 may be explained by models of $k_{\text{SF}} \sim 0.015$ (Gyr^{-1}). However, the gas mass fractions

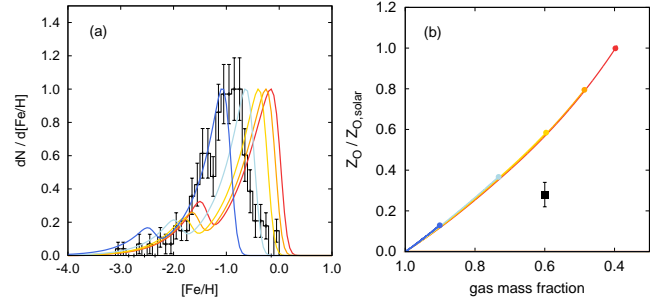


Figure 1. Comparisons between observational data of NGC 6822 and model A. The observed metallicity distribution (panel a) is taken from Kirby et al. (2013). For panel b, the gas mass fraction is derived based on the stellar mass from McConnachie (2012) and the gas mass (de Blok & Walter 2006; Israel 1997). The gas-phase oxygen abundance is from Lee et al. (2006) and is scaled to the solar value. For the observational data, see Sec. 2. The curves in the two panels are predictions from model A. The colours correspond to the SFE: blue, sky blue, yellow, orange and red curves show cases of $k_{\text{SF}} = 0.010, 0.030, 0.050, 0.070$ and 0.090 (Gyr^{-1}), respectively. Points in panel b are the predicted gas-phase oxygen abundance and gas mass fraction at present in the universe.

predicted by the models are larger than the observed value. Therefore, if NGC 6822 is a closed system, there may be physical processes in which heavy elements are not produced efficiently. One possibility is that the IMF is steeper than Salpeter's law (e.g. Lequeux et al. 1979; Matteucci & Chiosi 1983).

4.1.1 Cases of steeper IMF

If there is a system where star formation follows a steep IMF, massive stars are formed less frequently. Thus, a galaxy of a steeper IMF can have a lower average metallicity at a given gas fraction. Although it is not clear whether the IMF for dwarf galaxies differs from that for the solar neighbourhood, in this section the observational data of NGC 6822 are compared to model A under the assumption that star formation can obey a steeper IMF compared to that for the solar neighbourhood.

Figure 2 shows the metallicity distributions, gas-phase oxygen abundances and gas mass fractions of galaxies with different indices of IMF ($x = 1.35, 1.45$ and 1.55) and SFEs ($k_{\text{SF}} = 0.010, 0.050$ and 0.090 (Gyr^{-1})). Similar to the case of the Salpeter IMF, when the IMF is identical, galaxies evolve along almost self-similar tracks on the μ - Z_{O} diagram, regardless of the SFE. When galaxies of the same SFE but different IMFs are compared, galaxies of steeper IMFs have lower gas-phase oxygen abundances in the universe at present. Galaxies of steeper IMFs have slightly smaller present-day gas mass fractions, because more interstellar gas is locked in low-mass stars. With regard to the metallicity distributions, galaxies of steeper IMFs have lower $[\text{Fe}/\text{H}]_{\text{peak}}$. For example, a galaxy of $x = 1.55$ and $k_{\text{SF}} = 0.010$ (Gyr^{-1}) (thinnest blue curve in Fig. 2a) has a metallicity distribution of $[\text{Fe}/\text{H}]_{\text{peak}} \sim -1.4$, while the metallicity distribution of a galaxy of the same SFE but $x = 1.35$ (thickest blue curve) has $[\text{Fe}/\text{H}]_{\text{peak}} \sim -1.1$.

Fig. 2b suggests that the observed values of the gas mass fraction and gas-phase oxygen abundance may be explained

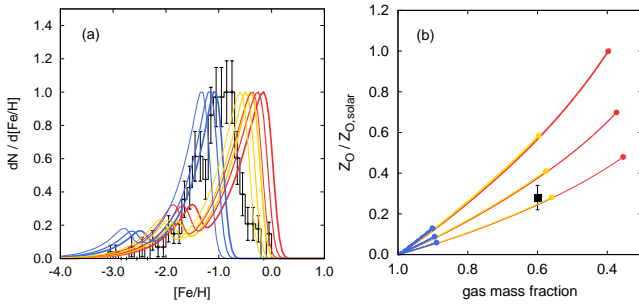


Figure 2. Metallicity distributions (panel a), gas-phase oxygen abundances and gas mass fractions (panel b) of galaxies of different IMFs and SFEs predicted by model A. Thinner curves indicate galaxies of steeper IMF. The index of IMF is varied by 0.10: $x = 1.35$ (thickest curves), 1.45 and 1.55 (thinnest curves). The colours of the curves correspond to the SFE: blue, yellow and red curves show galaxies of $k_{\text{SF}} = 0.010, 0.050$ and 0.090 (Gyr^{-1}), respectively. Points on the curves in panel b are present-day values. The black histogram and square in the panels are observational data presented in Sec. 2.

if the IMF is assumed to be $x \sim 1.50 - 1.55$. When the SFE is assumed to be $k_{\text{SF}} \sim 0.040 - 0.050$ (Gyr^{-1}), the observed values of gas-phase abundance and gas mass fraction can be consistent with the model predictions within the range of error. On the other hand, the metallicity distributions predicted by the models show higher $[\text{Fe}/\text{H}]_{\text{peak}}$ compared to the observed distribution and slightly underestimate stars of $[\text{Fe}/\text{H}] \sim 0$. These results suggest that if this galaxy is a closed system where steeper IMFs are allowed, it may be characterized by physical processes that are not assumed in model A, such as discontinuous star formation.

4.2 Accretion-dominated system

NGC 6822 is assumed to be a system where the accretion of primordial gas is dominant. The data are compared to model B.

Fig. 3 shows how the quantities predicted by model B vary with the SFE or the ACE when the Salpeter IMF is assumed. If different SFEs are applied while keeping the ACE fixed, similar trends to those of model A are seen (Figs. 3a–f). On the μ – Z_{O} plane, galaxies evolve along almost self-similar tracks.

When different ACEs are applied while keeping the SFE fixed (Figs. 3g–l), higher ACE results in the accretion of a larger fraction of gas in the reservoir in the early stage of the evolution, and stars are formed from the gas. Thus, if a galaxy has a high ACE, the metallicity distribution can have a slightly high $[\text{Fe}/\text{H}]_{\text{peak}}$ and high gas-phase oxygen abundance in the present universe. Galaxies of different ACEs evolve along almost self-similar tracks on the μ – Z_{O} diagram.

As it is known that the accretion of gas is one of solutions of the G-dwarf problem in the solar neighbourhood (e.g. Pagel & Patchett 1975), the overproduction of stars in the low-metallicity tail of metallicity distributions seems to be alleviated compared to model A. When the SFE is fixed (Figs. 3g, i and k), galaxies of smaller values of ACE/SFE have metallicity distributions of sharper main peaks, in the ranges of the SFE and ACE investigated in this study.

Galaxies of higher ACEs also tend to have stars of wider range of the metallicity.

As seen in the μ – Z_{O} diagrams in Fig. 3, model B predicts higher gas-phase oxygen abundances at the observed value of gas mass fraction of NGC 6822. For instance, a gas mass fraction predicted by a model of $k_{\text{SF}} = 0.050$ (Gyr^{-1}) and $k_{\text{in}} = 0.90$ (Gyr^{-1}) (yellow curves in Figs. 3e and f) is almost consistent with the observed value, but the model predicts higher gas-phase oxygen abundance and $[\text{Fe}/\text{H}]_{\text{peak}}$ compared to the observed values. Fig. 3 also suggests that there are cases where the observed gas-phase oxygen abundance and $[\text{Fe}/\text{H}]_{\text{peak}}$ can be explained (e.g. blue curves in Figs. 3i and j), but such models predict larger gas mass fractions compared to the observed value. Therefore, it seems that the observed values of gas-phase oxygen abundance and gas mass fraction are unlikely to be explained by different ACEs and SFEs alone.

4.2.1 Cases of steeper IMF

As described in Sec. 4.1.1, if star formation obeys a steep IMF, the galaxy may have lower gas-phase oxygen abundance at a fixed gas fraction. In this section, the observational data are compared to model B under the assumption that star formation obeys steeper IMFs compared to the Salpeter IMF.

Figure 4 shows the properties of galaxies of different SFEs, ACEs and IMFs. Generally, at a fixed IMF, the trends are similar to those in the case of the Salpeter IMF. In the μ – Z_{O} diagrams, galaxies evolve along almost self-similar tracks, regardless of the SFE or ACE. When galaxies have the same SFE and ACE, galaxies of steeper IMFs have lower gas-phase oxygen abundances at a given gas mass fraction and metallicity distributions of lower $[\text{Fe}/\text{H}]_{\text{peak}}$.

In the μ – Z_{O} diagrams shown in Fig. 4, the observed values of NGC 6822 seem to be explained if the slope of IMF is assumed to be $x \sim 1.50 - 1.55$ (see also Appendix B for details). This result may not disagree with those of a study by Gavilán et al. (2013), who suggest that the gas-phase oxygen abundances and gas fractions of dwarf irregular galaxies can be explained by the infall model in which no outflow is included. On the other hand, the models that can explain the gas-phase oxygen abundance and gas mass fraction predicts a metallicity distribution of higher $[\text{Fe}/\text{H}]_{\text{peak}}$ compared to the observed distribution.

In summary, if steeper IMFs are allowed, the observed values of gas mass fraction and gas-phase oxygen abundance can be explained by model B. On the other hand, metallicity distributions predicted by the models tend to have higher $[\text{Fe}/\text{H}]_{\text{peak}}$ and the shape of the observed distribution cannot be explained. If NGC 6822 is an accretion-dominated system, there may be dominant physical processes that are not taken into account in model B. Although the literature suggests that more massive irregular galaxies are likely to have more continuous star formation histories (Tosi 1998; Weisz et al. 2012), assuming fluctuations in gas accretion and multiple starbursts may explain the metallicity distribution of NGC 6822 (Hartwick 2015).

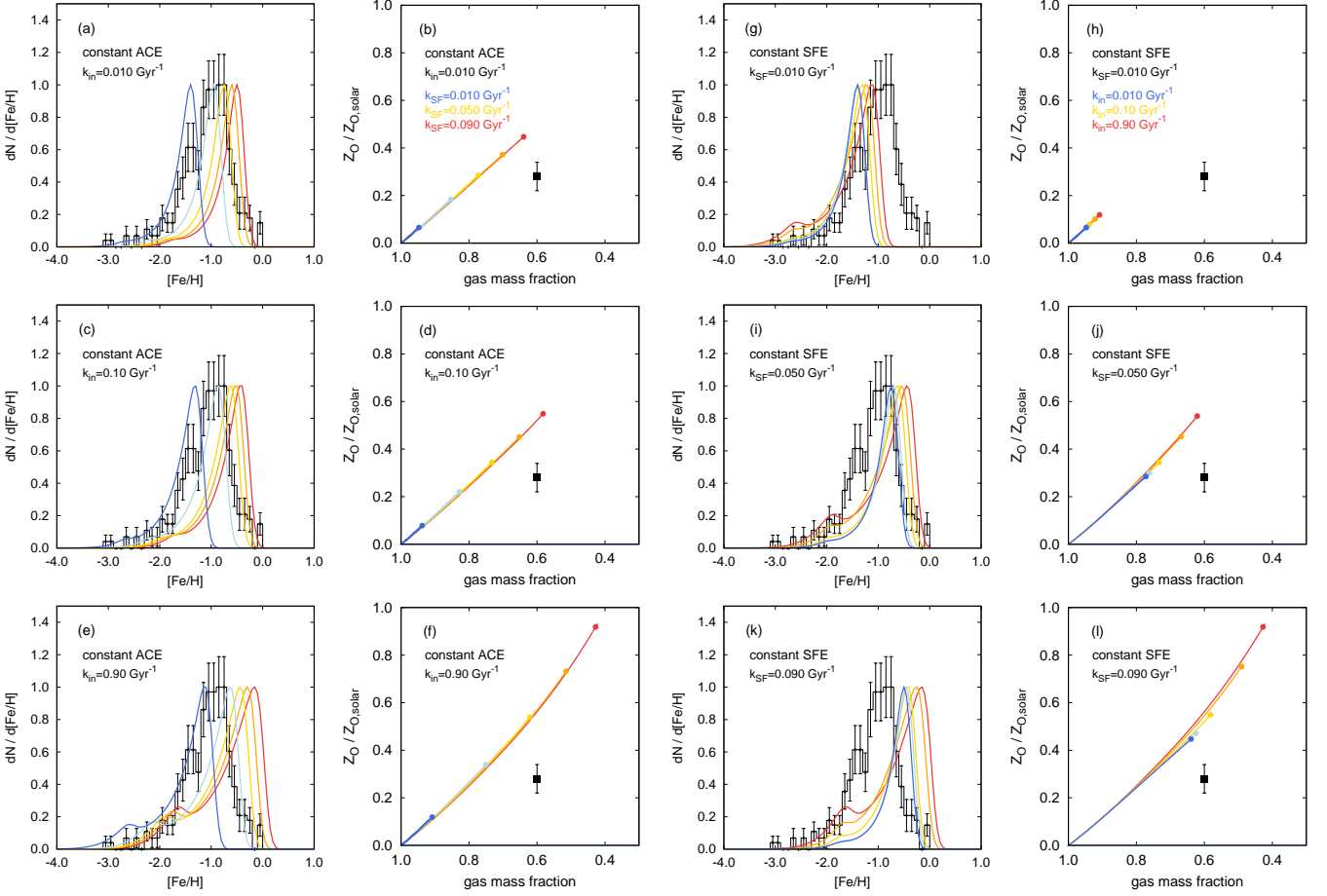


Figure 3. Comparisons between the observational data (black histograms and squares; see Sec. 2 for the references) and model B. The Salpeter IMF ($x = 1.35$) is assumed. (a)–(f) Cases of different SFEs while the ACE is fixed. The colours of the curves correspond to the SFE: blue, sky blue, yellow, orange and red curves are cases of $k_{\text{SF}} = 0.010, 0.030, 0.050, 0.070$ and 0.090 (Gyr^{-1}), respectively. The values of the ACE are $k_{\text{in}} = 0.010$ (panels a and b), 0.10 (c and d) and 0.90 (Gyr^{-1}) (e and f). (g)–(l) Cases of different ACEs while the SFE is fixed. The colours of the curves correspond to the ACE: blue, sky blue, yellow, orange and red curves are cases of $k_{\text{in}} = 0.010, 0.032, 0.10, 0.32$ and 0.90 (Gyr^{-1}), respectively. The values of the SFE are $k_{\text{SF}} = 0.010$ (panels g and h), 0.050 (i and j) and 0.090 (Gyr^{-1}) (k and l). Points on the curves show the gas-phase oxygen abundances and gas mass fractions in the universe at present.

4.3 Outflow-dominated system

NGC 6822 is assumed to be a system in which the outflow is dominant. Model C is compared to the data and the Salpeter IMF is assumed.

Fig. 5 shows how quantities predicted by model C vary based on the SFE (Figs. 5a–f) or the mass-loading factor (Figs. 5g–l). When galaxies of different SFEs are compared, galaxies of higher SFE have a smaller gas mass fraction and higher gas-phase oxygen abundance in the present universe (Figs. 5b, d and f). When the mass-loading factor is fixed, galaxies evolve along almost self-similar tracks on the μ – Z_{O} plane, regardless of the SFE.

In addition, as shown in Figs. 5g–l, galaxies of larger mass-loading factor have lower gas-phase oxygen abundances at a given gas mass fraction (Hartwick 1976; Pagel 1997). If a galaxy has a larger mass-loading factor, the gas of that galaxy is expelled more efficiently, resulting in a smaller gas mass fraction in the universe at present (Figs. 5h, j and l). With regard to metallicity distributions, galaxies of larger mass-loading factors tend to have lower $[\text{Fe}/\text{H}]_{\text{peaks}}$ (Fig. 5k).

The metallicities of the most metal-rich stars seem to be almost consistent among galaxies of different mass-loading factors.

The trends shown in Fig. 5 suggest that the observed gas-phase oxygen abundance at the gas mass fraction of NGC 6822 can be explained by models of $\eta \gtrsim 3$ (Fig. 5d). If the SFE is too low, a galaxy has a large gas mass fraction and low gas-phase oxygen abundance in the universe at present compared to the observed values. On the other hand, if the SFE is high, a galaxy evolves rapidly, resulting in a small gas mass fraction and high gas-phase oxygen abundance. Thus, the range of SFE is also roughly constrained.

In Fig. 6, the case of $\eta = 6.0$ and $k_{\text{SF}} = 0.020$ (Gyr^{-1}) is examined as an example. The gas mass fraction and gas-phase oxygen abundance are almost consistent with the values predicted by the model (Fig. 6b). The predicted metallicity distribution is also roughly consistent with the observed distribution within the margin of error in the metallicity range of $[\text{Fe}/\text{H}] \sim -2.0$ to -0.5 . The values of the mass-loading factor that explain the observational data are not markedly different from those suggested by other theoretic

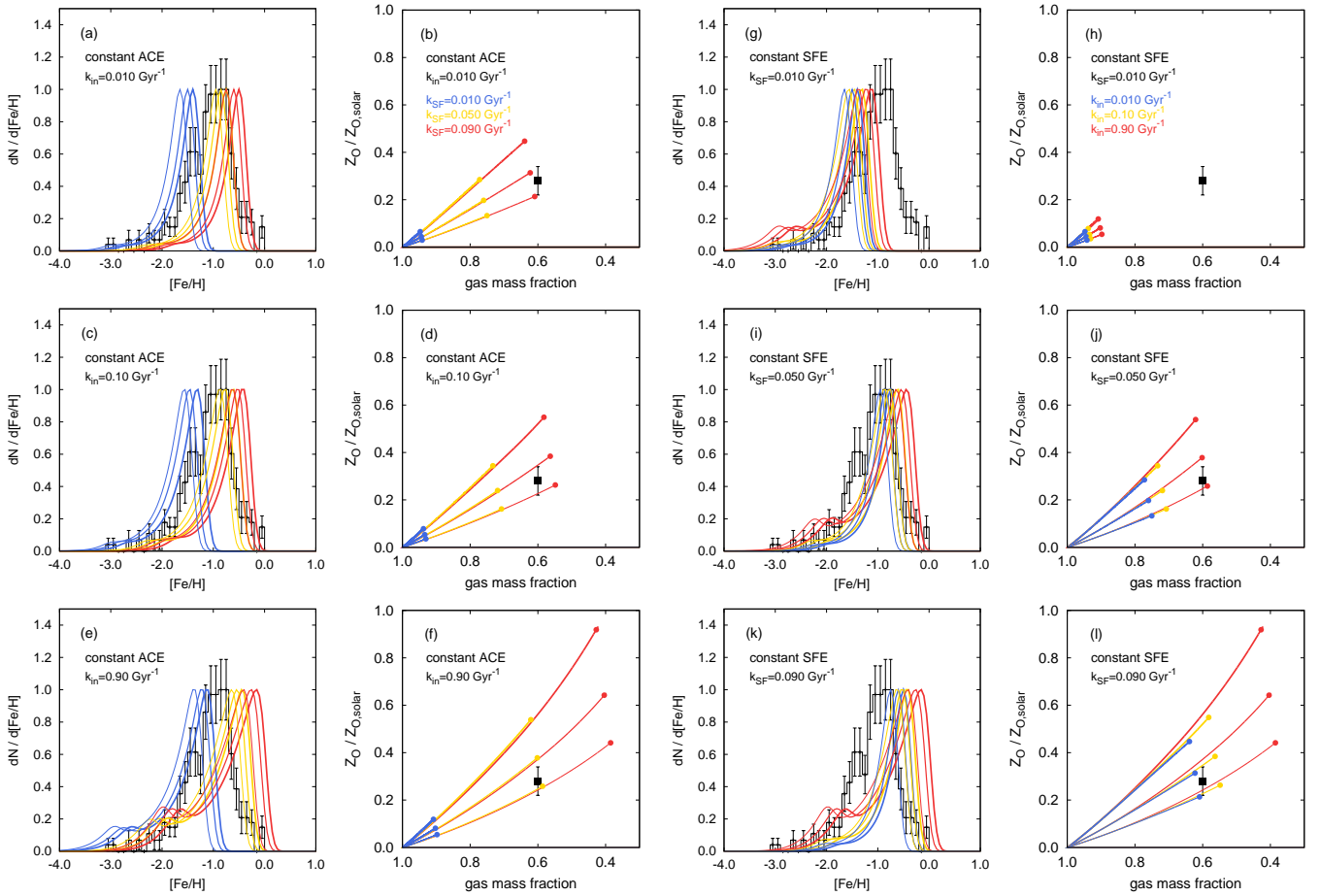


Figure 4. Metallicity distributions, gas-phase oxygen abundances and gas mass fractions of galaxies of different IMFs, SFEs and ACEs predicted by model B. Thinner curves show galaxies of steeper IMF. The index of IMF is varied by 0.10: $x = 1.35$ (thickest curves), 1.45 and 1.55 (thinnest curves). (a)–(f) Cases of different SFEs while the ACE is fixed. The colours of the curves correspond to the SFE: blue, yellow and red curves show galaxies of $k_{SF} = 0.010, 0.050$ and 0.090 Gyr^{-1} , respectively. The ACE is assumed to be $k_{in} = 0.010$ (panels a and b), 0.10 (c and d) and $0.90 \text{ (Gyr}^{-1})$ (e and f). (g)–(l) Cases of different ACEs while the SFE is fixed. The colours of the curves correspond to the value of the ACE: blue, yellow and red curves show galaxies of $k_{in} = 0.010, 0.10$ and 0.90 Gyr^{-1} , respectively. The SFE is assumed to be $k_{SF} = 0.010$ (panels g and h), 0.050 (i and j) and $0.090 \text{ (Gyr}^{-1})$ (k and l). Points on the curves in the μ – Z_O diagrams show the present-day values. Black histograms and squares in the panels are the observational data presented in Sec. 2.

cal studies using simulations (e.g. $3 \lesssim \eta \lesssim 10$ for galaxies of $M_* \sim 10^8 M_\odot$, Muratov et al. 2017).

In summary, the gas-phase oxygen abundance, gas mass fraction and metallicity distribution ($-2.0 \lesssim [\text{Fe}/\text{H}] \lesssim -0.5$) can be roughly explained by model C, in which continuous star formation and outflow are assumed. Thus, if NGC 6822 is an outflow-dominated system, the history of star formation and outflow of this galaxy may be continuous. Meanwhile, it should be noted that the present study is based on the simplified models. In model C, it is assumed that a galaxy is formed from a gas cloud, while observations suggest the accretion of other systems, such as dwarf galaxies (e.g. Hwang et al. 2014). More importantly, model C generally overproduces stars of $[\text{Fe}/\text{H}] \lesssim -2$ (Fig. 6). As discussed in Sec. 4.2 and previous studies (e.g. Pagel & Patchett 1975; Prantzos 2003), the gas accretion may alleviate the overproduction. Thus, outflow may be a dominant process, but other physical processes, including the accretion of gas or gas-rich systems, are not completely excluded. For further investigation of the history of star formation and gas flows,

detailed modellings and observational information, such as stellar abundance ratios, are needed.

4.4 Caveats

It should be noted that observational data are compared to models with a few assumptions. In the models, SNe II and SNe Ia are assumed to be the main contributors to chemical enrichment, but it is possible that other events e.g. hypernovae or different types of supernovae, affect the enrichment of oxygen and iron. The assumptions about SNe Ia are also oversimplified. The lifetime and fraction of the progenitors are assumed to be fixed values. Relaxation of these assumptions may result in different values of predicted gas-phase and stellar abundances, and thus lead to different conclusions. In addition, the significance of dust depletion in a low-metallicity environment is still unclear. Additional observational and theoretical data are required.

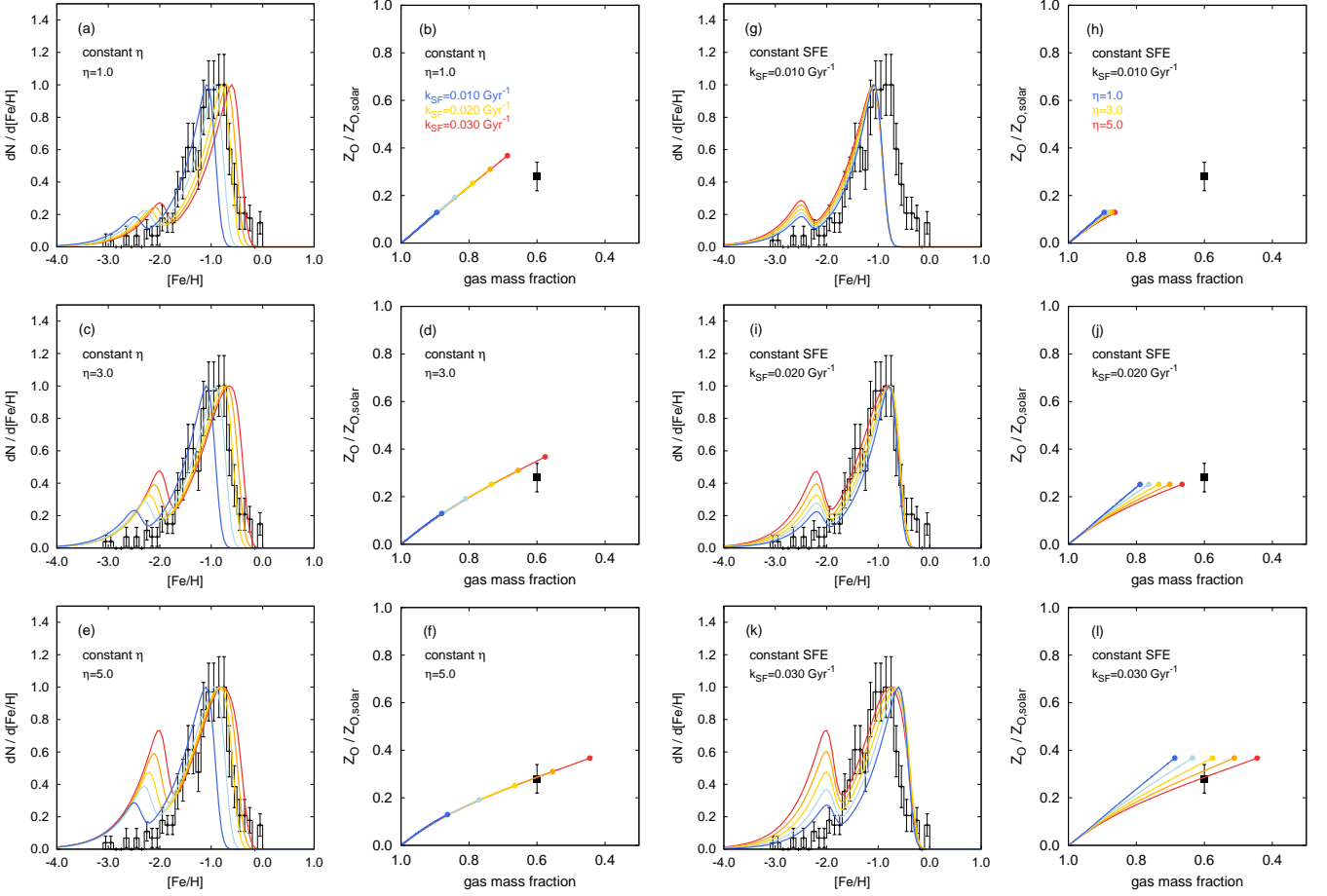


Figure 5. Comparisons between the observational data (black histograms and squares, see Sec. 2 for references) and model C. The Salpeter IMF ($x = 1.35$) is assumed. (a)–(f) Cases of different SFEs while the mass-loading factor is fixed. The colours of the curves correspond to the SFE: blue, sky blue, yellow, orange and red curves are cases of $k_{\text{SF}} = 0.010, 0.015, 0.020, 0.025$ and 0.030 (Gyr^{-1}), respectively. The values of the mass-loading factor are $\eta = 1.0$ (panels a and b), 3.0 (c and d) and 5.0 (e and f). (g)–(l) Cases of different mass-loading factors while the SFE is fixed. The colours of the curves correspond to the mass-loading factor: blue, sky blue, yellow, orange and red curves are cases of $\eta = 1.0, 2.0, 3.0, 4.0$ and 5.0, respectively. The values of the SFE are $k_{\text{SF}} = 0.010$ (panels g and h), 0.020 (i and j) and 0.030 (Gyr^{-1}) (k and l). Points on the curves show the gas-phase oxygen abundances and gas mass fractions in the universe at present.

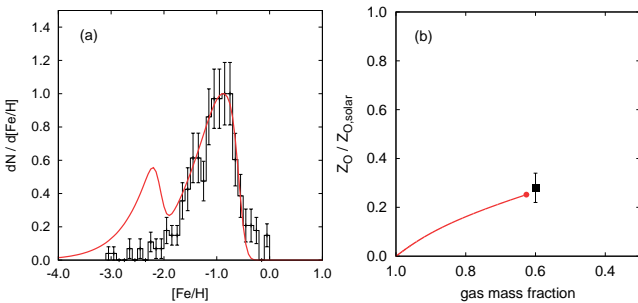


Figure 6. Same as Fig. 5, but the case of $\eta = 6.0$ (red curves) is investigated. The SFE is assumed to be $k_{\text{SF}} = 0.020$ (Gyr^{-1}).

5 SUMMARY AND DISCUSSION

This paper discusses the chemical evolution of a dwarf irregular galaxy in the Local Group NGC 6822 from the viewpoints of gas-phase and stellar abundances. Observed gas-phase oxygen abundance, gas mass fraction and stellar

metallicity distribution are compared to chemical evolution models in which continuous star formation, gas accretion and/or outflow are taken into account.

In the cases of the closed-box and infall models, the gaseous properties can be explained if steeper IMFs are allowed. On the other hand, the shapes of the metallicity distributions predicted by the models are not consistent with the observed distribution, suggesting that the galaxy has a more complex history of star formation, gas flows and/or chemical enrichment than assumed in the models.

When the observational data are compared to the outflow model, the observed values of gas-phase oxygen abundance and gas mass fraction can be explained. The shape of the observed metallicity distribution is also roughly consistent with those predicted by some of the models in the metallicity range of $-2.0 \lesssim [\text{Fe}/\text{H}] \lesssim -0.5$. Thus, if NGC 6822 is an outflow-dominated system, the history of star formation and outflow may be continuous. This result does not mean that the accretion of gas or gas-rich systems is completely excluded. For further discussion about the history of

star formation and gas flows, additional observables and detailed modelling are needed. Because stars of different properties (e.g. mass) contribute to the enrichment of different elements, stellar abundance ratios may give insight into the star formation history. With regard to the observed stellar metallicity, the shape of metallicity distributions might be different if the sample size and the method of metallicity measurement are different (Swan et al. 2016). More spectroscopic data will help understand dominant physical processes that affect the chemical evolution.

Finally, each dwarf galaxy has a unique star formation history, so studies of other dwarf irregular galaxies from the viewpoints of gas-phase and stellar metallicities may provide further insight into the variation in the star formation and gas flow histories.

ACKNOWLEDGEMENTS

Sincere thanks are due to Dr. Yuhri Ishimaru, who passed away in November 2017. This study has been developed from a study conducted under her guidance. The reviewer's comments have also greatly improved the manuscript.

REFERENCES

- Adibekyan V. Zh., Santos N. C., Sousa S. G., Israelian G., 2011, *A&A*, 535L, 11
- Adibekyan V. Zh., Sousa S. G., Santos N. C., Delgado Mena E., González Hernández J. I., Israelian G., Mayor M., Khachatryan G., 2014, *A&A*, 545A, 32
- Asplund M., Grevesse N., Sauval A. J., Allende Prieto C., Kiselman D., 2004, *A&A*, 417, 751
- Bensby T., Feltzing S., Oey M. S., 2014, *A&A*, 562A, 71
- Cannon J. M., et al., 2012, *ApJ*, 747, 122
- Carigi L., Colín P., Peimbert M., 2006, *ApJ*, 644, 924
- Carney B. W., Aguilar L. A., Latham D. W., Laird J. B., 2005, *AJ*, 129, 1886
- Colucci J. E., Bernstein R. A., McWilliam A., 2010,
- de Blok W. J. G., Walter F., 2006, *AJ*, 131, 343
- Fusco F., Buonanno R., Hidalgo S. L., Aparicio A., Pietrinferni A., Bono G., Monelli M., Cassisi S., 2014, *A&A*, 572A, 26
- Gavilán M., Ascasibar Y., Mollá M., Díaz Á. I., 2013, *MNRAS*, 434, 2491
- Hartwick F. D. A., 1976, *ApJ*, 209, 418
- Hartwick F. D. A., 2015, *AJ*, 150, 184
- Hernández-Martínez L., Peña M., Carigi L., García-Rojas J., 2009, *A&A*, 505, 1027
- Hernández-Martínez L., Carigi L., Peña M., Peimbert M., 2011, *A&A*, 535A, 118
- Hunter D. A., Elmegreen B. G., 2004, *AJ*, 128, 2170
- Hwang N., Park H. S., Lee M. G., Lim S., Hodge P. W., Kim S. C., Miller B., Weisz D., 2014, *ApJ*, 783, 49
- Israel F. P., 1997, *A&A*, 317, 65
- Israel F. P., Bontekoe T. R., Kester D. J. M., 1996, *A&A*, 308, 723
- Kirby E. N., Cohen J. G., Guhathakurta P., Cheng L., Bullock J. S., Gallazzi A., 2013, *ApJ*, 779, 102
- Kirby E. N., et al., 2019, *ApJ*, 881, 45
- Kroupa P., 2001, *MNRAS*, 322, 231
- Larsen S. S., Brodie J., Wasserman A., Strader J., 2018, *A&A*, 613A, 56
- Leaman R., et al., 2013, *ApJ*, 767, 131
- Lee H., Skillman E. D., Venn K. A., 2006, *ApJ*, 642, 813
- Lian J., Thomas D., Maraston C., Goddard D., Comparat J., Gonzalez-Perez V., Ventura P., 2018, *MNRAS*, 474, 1143
- Lequeux J., Peimbert M., Rayo J. F., Serrano A., Torres-Peimbert S., 1979, *A&A*, 80, 155
- Mateo M. L., 1998, *ARA&A*, 36, 435
- Matteucci F., 2012, *Chemical Evolution of Galaxies*. Springer-Verlag, Berlin
- Matteucci F., Chiosi C., 1983, *A&A*, 123, 121
- McConnachie A. W., 2012, *AJ*, 144, 4
- Muratov A. L., et al., 2017, *MNRAS*, 468, 4170
- Muschielok M., et al., 1999, *A&A*, 352L, 40
- Nomoto K., Iwamoto K., Nakasato N., Thielemann F.-K., Brachwitz F., Tsujimoto T., Kubo Y., Kishimoto N., 1997, *Nuclear Phys. A*, 621, 467
- Nomoto K., Kobayashi C., Tominaga N., 2013, *ARA&A*, 51, 457
- Pagel B. E. J., 1997, *Nucleosynthesis and Chemical Evolution of Galaxies*. Cambridge University Press, Cambridge
- Pagel B. E. J., Patchett B. E., 1975, *MNRAS*, 172, 13
- Patrick L. R., Evans C. J., Davies B., Kudritzki R.-P., Gazak J. Z., Bergemann M., Plez B., Ferguson A. M. N., 2015, *ApJ*, 803, 14
- Peimbert A., Peimbert M., Ruiz M. T., 2005, *ApJ*, 634, 1056
- Prantzos N., 2003, *A&A*, 404, 211
- Prantzos N., 2008, in Charbonnel C., Zahn J. P., eds, *EAS Publication Series, Vol. 32, Stellar Nucleosynthesis: 50 years after B²FH*. EDP Sciences, p. 311
- Prantzos N., Abia C., Limongi M., Chieffi A., Cristallo S., 2018, *MNRAS*, 476, 3432
- Revaz Y., Jablonka P., 2018, *A&A*, 616A, 96
- Richer M. G., McCall M. L., 2007, *ApJ*, 658, 328
- Roederer I. U., Preston G. W., Thompson I. B., Shectman S. A., Sneden C., Burley G. S., Kelson D. D., 2014, *AJ*, 147, 136
- Salpeter E. E., 1955, *ApJ*, 121, 161
- Schaller G., Schaerer D., Meynet G., Maeder A., 1992, *A&AS*, 96, 269
- Skillman E. D., Terlevich R., Melnick J., 1989, *MNRAS*, 240, 563
- Swan J., Cole A. A., Tolstoy E., Irwin M. J., 2016, *MNRAS*, 456, 4315
- Tautvaišienė G., Geisler D., Wallerstein G., Borissova J., Bizyaev D., Pagel B. E. J., Charbonnel C., Smith V., 2007, *AJ*, 134, 2318
- Tolstoy E., Irwin M. J., Cole A. A., Pasquini L., Gilmozzi R., Gallagher J. S., 2001, *MNRAS*, 327, 918
- Tolstoy E., Hill V., Tosi M., 2009, *ARA&A*, 47, 371
- Tosi M., 1998, in Thuan T. X., Balkowski C., Cayatte V., Tran Than Van J., eds, *XVIIIth Rencontre de Moriond*
- Tsujimoto T., Nomoto K., Yoshii Y., Hashimoto M., Yanagida S., Thielemann F.-K., 1995, *MNRAS*, 277, 945
- Venn K. A., et al., 2001, *ApJ*, 547, 765
- Venn K. A., Irwin M., Shetrone M. D., Tout C. A., Hill V., Tolstoy E., 2004, *AJ*, 128, 1177
- Weisz D. R., et al., 2012, *ApJ*, 744, 44
- Weisz D. R., Dolphin A. E., Skillman E. D., Holtzman J., Gilbert K. M., Dalcanton J. J., Williams B. F., 2014, *ApJ*, 789, 147
- Yoshii Y., Tsujimoto T., Nomoto K., 1996, *ApJ*, 462, 266

APPENDIX A: THE FRACTION AND LIFETIME OF PROGENITORS OF TYPE-IA SUPERNOVAE

Although it is possible that the mechanisms of SNe Ia differ among galaxies (e.g. Kirby et al. 2019), it is still not clear whether or how the mechanism of SNe Ia varies from galaxy to galaxy. In the metallicity range of $-2.5 \lesssim [\text{Fe}/\text{H}] \lesssim 0$, the binary fraction of field stars may not significantly varied with

the metallicity (Carney et al. 2005). In this study, the fraction f_{Ia} and the lifetime τ_{Ia} in models A–C are determined based on the assumption that the mechanism of SNeIa in dwarf galaxies is not significantly different from that in the Milky Way.

The accretion of gas may be one way in which the metallicity distribution of long-lived stars in the solar neighbourhood can be explained (e.g. Pagel & Patchett 1975). Assuming that the formation of the thin disc of the Milky Way is dominated by the accretion of primordial gas, the metallicity distribution of long-lived stars in the thin disc and stellar abundance ($[\text{Mg}/\text{Fe}]$) of the Milky Way are compared to the infall model (model B). The one-zone model is probably too simple to completely reproduce the observational data of the Milky Way (Prantzos et al. 2018). Previous studies have indicated that there are two or three families of stars on the $[\text{Mg}/\text{Fe}]$ – $[\text{Fe}/\text{H}]$ plane at $[\text{Fe}/\text{H}] \gtrsim -0.7$ (e.g. Adibekyan et al. 2011), and their origins are still a matter of debate. In this study, τ_{Ia} and f_{Ia} are determined, and trends of the observational data are broadly explained using model B. With regard to the $[\text{Mg}/\text{Fe}]$ – $[\text{Fe}/\text{H}]$ diagram, it is assumed that α -elements are produced mainly by massive stars in the early stages of evolution, and then $[\text{Mg}/\text{Fe}]$ begins to decline due to the enrichment of Fe by SNeIa.

Fig. A1 shows how the metallicity distribution and $[\text{Mg}/\text{Fe}]$ can be varied by τ_{Ia} and f_{Ia} . Figs. A1a and b show the case where different τ_{Ia} are assumed while f_{Ia} is fixed. As shown in the $[\text{Mg}/\text{Fe}]$ – $[\text{Fe}/\text{H}]$ diagram, $[\text{Mg}/\text{Fe}]$ starts to decline at higher $[\text{Fe}/\text{H}]$ with longer τ_{Ia} . In model B, when the lifetime of progenitors of SNeIa is set to τ_{Ia} (Gyr), the first SNIa explosion occurs τ_{Ia} Gyr after star formation starts in the system. Until the first SNIa explodes, the chemical enrichment proceeds by SNeII. Therefore, if τ_{Ia} is assumed to be longer, the metallicity at the time when SNeIa starts to contribute to the chemical enrichment can be high. This effect also causes a larger number of stars of $[\text{Fe}/\text{H}] \sim -1.0$ in metallicity distributions for cases of longer τ_{Ia} (Fig. A1a).

Figs. A1c and d show cases where f_{Ia} is varied while τ_{Ia} is fixed. If f_{Ia} is large, the number of SNeIa is also large, resulting in more enrichment of Fe by SNeIa. Thus, if a larger f_{Ia} is assumed, the $[\text{Fe}/\text{H}]$ at the peak of metallicity distributions is high (Fig. A1c). In addition, larger f_{Ia} is associated with more significant declines in $[\text{Mg}/\text{Fe}]$ at $[\text{Fe}/\text{H}] \gtrsim -1.0$ in the $[\text{Mg}/\text{Fe}]$ – $[\text{Fe}/\text{H}]$ diagram (Fig. A1d).

The curves shown in Figs. A2a and b are predictions made by model B, where $\tau_{\text{Ia}} = 2.0$ (Gyr), $f_{\text{Ia}} = 0.05$, $k_{\text{SF}} = 0.42$ (Gyr^{-1}) and $k_{\text{in}} = 0.10$ (Gyr^{-1}). This model broadly explains the shape of the metallicity distribution (for the overproduction of metal-poor stars, see Sec. 3.1), the metallicity around the point where $[\text{Mg}/\text{Fe}]$ starts to decline ($[\text{Fe}/\text{H}] \sim -1$) and the solar abundance ($[\text{Mg}/\text{Fe}] \sim [\text{Fe}/\text{H}] \sim 0$). The gas to stellar fraction predicted by the model is also consistent with that of the Milky Way (about 0.1–0.15). These values of the model are roughly within the ranges suggested in the literature (e.g. Yoshii, Tsujimoto & Nomoto 1996). Based on these observations, it is assumed that 5 per cent of stars of 3–8 M_{\odot} explode as SNeIa 2 Gyr after their formation. The observational data can also be explained by different values of τ_{Ia} and f_{Ia} , such as $\tau_{\text{Ia}} = 1.5$ (Gyr) and $f_{\text{Ia}} = 0.05$, but if the Kroupa IMF (Kroupa 2001) is adopted, $\tau_{\text{Ia}} = 2.0$ (Gyr) and $f_{\text{Ia}} = 0.05$ are preferred. The variations in the lifetime and fraction with IMF are not clear, so this

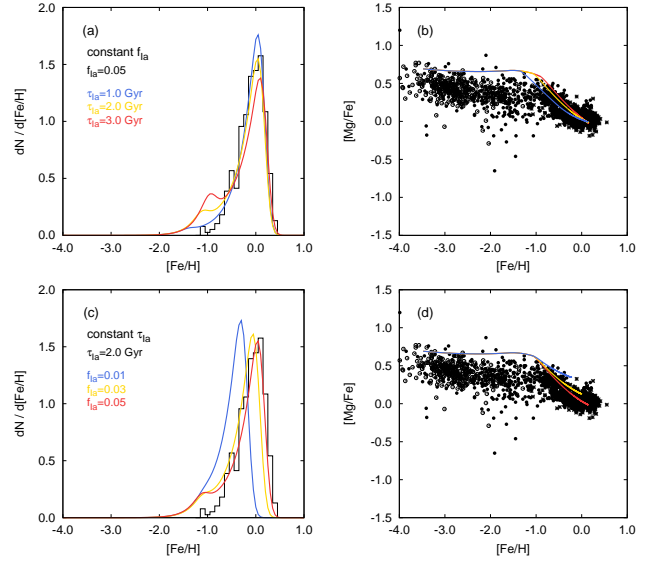


Figure A1. Metallicity distributions (panels a and c) and $[\text{Mg}/\text{Fe}]$ (b and d) predicted by model B. (Panels a and b) The case where the lifetime of progenitors of SNeIa τ_{Ia} is varied while the fraction f_{Ia} is fixed at $f_{\text{Ia}} = 0.05$. Blue, yellow and red curves show cases of $\tau_{\text{Ia}} = 1.0, 2.0$ and 3.0 (Gyr), respectively. (Panels c and d) The case where f_{Ia} is varied while τ_{Ia} is fixed at $\tau_{\text{Ia}} = 2.0$ (Gyr). Blue, yellow and red curves show cases of $f_{\text{Ia}} = 0.01, 0.03$ and 0.05 . For all panels, the SFE and ACE are assumed to be $k_{\text{SF}} = 0.40$ (Gyr^{-1}) and $k_{\text{in}} = 0.10$ (Gyr^{-1}), respectively. The Salpeter IMF is assumed. The black histograms in panels a and c show the observed metallicity distribution, as reported by Bensby, Feltzing & Oey (2014). Data of $[\text{Mg}/\text{Fe}]$ of individual stars in the Milky Way (panels b and d) are taken from Venn et al. (2004, dots), Roederer et al. (2014, open circles) and Adibekyan et al. (2012, asterisks).

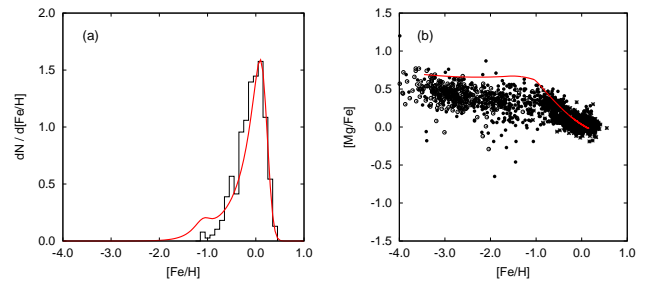


Figure A2. Same as Fig. A1, but comparing a model of $\tau_{\text{Ia}} = 2.0$ (Gyr), $f_{\text{Ia}} = 0.05$, $k_{\text{SF}} = 0.42$ (Gyr^{-1}) and $k_{\text{in}} = 0.10$ (Gyr^{-1}) (red curves) to observational data. The Salpeter IMF is adopted. The data are the same as in Fig. A1.

study assumes that these quantities are not correlated with IMF, and that these quantities are the same in the Milky Way and other galaxies.

As seen in Fig. A1a, $[\text{Fe}/\text{H}]_{\text{peak}}$ of metallicity distributions seems not to be greatly varied with τ_{Ia} . While the assumption about τ_{Ia} is simple, other uncertainty included in the models, e.g. assumptions about the chemical enrichment, may more greatly affect the general results of this study.

APPENDIX B: COMPARISON BETWEEN THE OBSERVATIONAL DATA AND MODEL B

Fig. B1 compares the observational data to models of $x = 1.50$ (Figs. B1a–j) and 1.55 (Figs. B1k–t) in detail. As explained in Sec. 4.2, the observed values of the gas-phase oxygen abundance and gas mass fraction of NGC 6822 can be explained by model B, if steeper IMFs are allowed. For example, the observed values are consistent with models of $x = 1.50$, $k_{\text{SF}} = 0.050 \text{ Gyr}^{-1}$ and $k_{\text{in}} \sim 0.70 \text{ Gyr}^{-1}$ within the margin of error for the observed gas-phase oxygen abundance (orange curve and point in Fig. B1f). However, the shape of the metallicity distributions predicted by the models seem not to be consistent with the observed distribution. Similar trends can be seen in Fig. B1 for other models.

This paper has been typeset from a $\text{\TeX}/\text{\LaTeX}$ file prepared by the author.

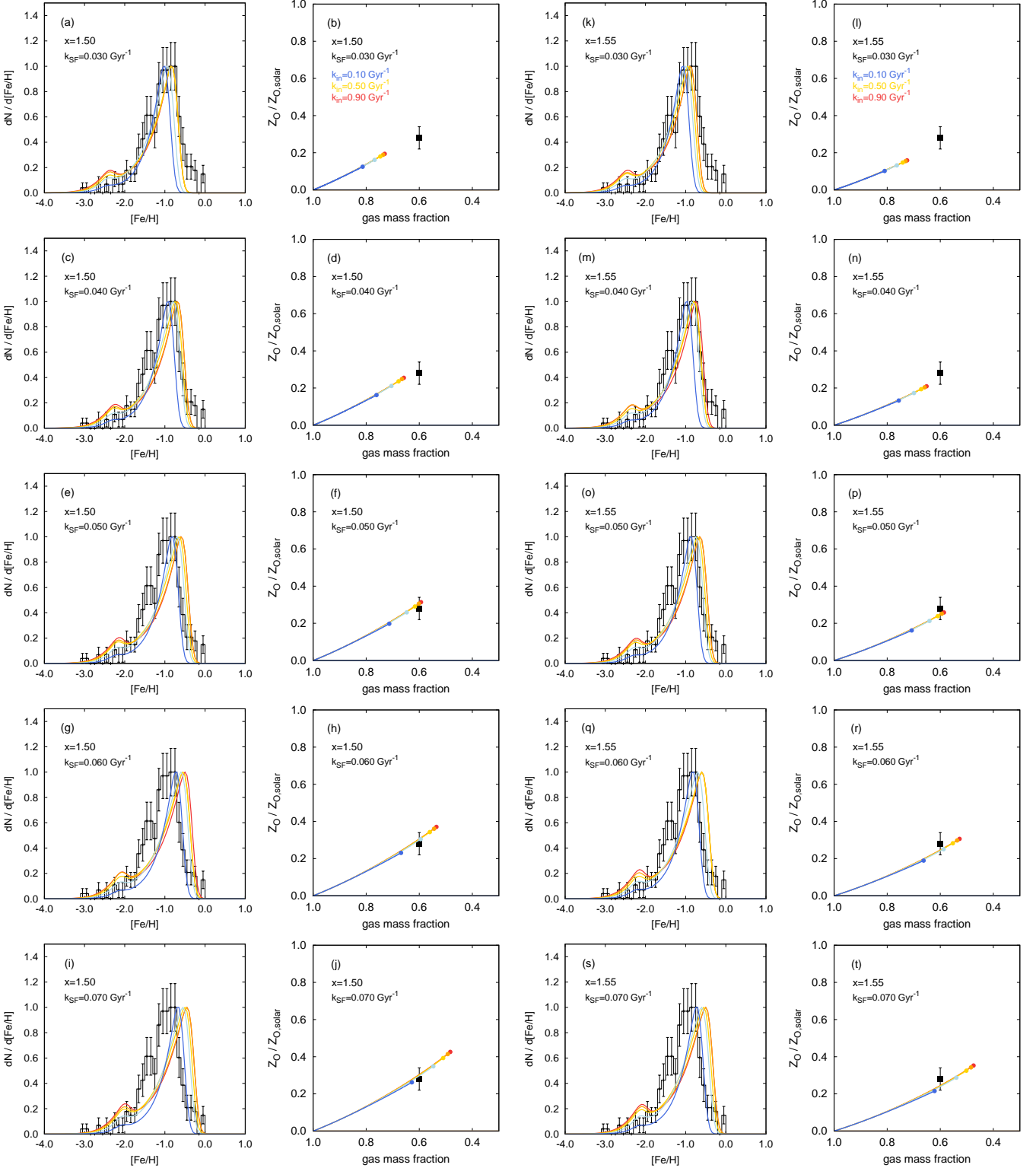


Figure B1. Comparison between observational data and model B. Cases of $x = 1.50$ and $x = 1.55$ are examined in detail. (a)–(j) Cases of $x = 1.50$. SFEs are $k_{\text{SF}} = 0.030$ (panels a and b), 0.040 (c and d), 0.050 (e and f), 0.060 (g and h) and 0.070 (Gyr^{-1}) (i and j). The colours of the curves correspond to the value of the ACE: blue, sky blue, yellow, orange and red curves show cases of $k_{\text{in}} = 0.10, 0.30, 0.50, 0.70$ and 0.90 (Gyr^{-1}), respectively. (k)–(t) Cases of $x = 1.55$. The SFE is assumed to be $k_{\text{SF}} = 0.030$ (panels k and l), 0.040 (m and n), 0.050 (o and p), 0.060 (q and r) and 0.070 (Gyr^{-1}) (s and t). ACEs of the models are the same as those for the case $x = 1.50$. Points on the curves in the μ – Z_0 diagrams represent the present-day values. Black histograms and squares in the panels are observational data presented in Sec. 2.